

# Turbulent Modeling Effects on Finite Volume Solution of Three Dimensional Aerated Hydraulic Jumps using Volume of Fluid

SAEED-REZA SABBAGH-YAZDI\*, FATEMEH ROSTAMI\*\*

Civil Engineering Department,  
KN Toosi University of Technology,  
No.1346 Valiasr Street, 19697- Tehran, IRAN

---

NIKOS E. MASTORAKIS

Military Institutes of University Education (ASEI)  
Hellenic Naval Academy  
Terma Chatzikyriakou 18539, Piraeus, GREECE

---

*Abstract:* This paper aims at characterizing the turbulent flow in hydraulic jumps. The paper starts by giving briefly insight into the dynamics of the flow and discussing mathematical description of aerated flow as well as the turbulent models which are suitable for numerical solution of hydraulic jump. The numerical models, which include an algorithm for air entrainment, have been implemented in a finite volume flow solver. Numerical simulations undertaken in present three dimensional work use  $k-\varepsilon$  and  $RNG$  turbulent models. Results are compared with observations of mean flow (Chanson & Brattberg 2000 and S. Wu & N. Rajaratnam 1996).

*Key-Words:* Numerical Simulation, Hydraulic Jumps, Air-Entrainment, Volume of Fluid (VOF and FAVOR).

## 1 Introduction

In open channels, the transition between supercritical and sub-critical flow (i.e. a hydraulic Jump) is characterized by a sharp rise in free-surface elevation, strong turbulence, water splashing and air entrainment in the roller.

Historically air entrainment in hydraulic jump was experimentally investigated in terms of the air demand: i.e., the total quantity of entrained air (e.g. Wood, 1990; Chanson, 1997). A 'milestone' contribution was the work of Resch and Leutheusser (1972) who showed first that the air entrainment process, the transfer of momentum and the energy dissipation are strongly affected by the inflow conditions. Recently, Chanson studied particularly the air-water properties in partially-developed hydraulic jumps and he showed a similarity with plunging jet entrainment (Chanson and Qiao, 1994; Chanson, 1995).

The outstanding features of hydraulic jumps can be summarized as follows: a) important turbulence intensities (often called macro turbulence); b) strong curvature of streamlines (i.e., non-hydrostatic pressure distribution); c) noticeable air entrainment into the water column through the free surface; and d) presence of a

roller of horizontal axis in the upper portion of the flow.

In spite of the general impression that the hydraulic jump is a well-known flow phenomenon, detailed theoretical and numerical models of all the internal flow features in hydraulic jumps, for all Froude numbers, have yet to be developed.

Some of the few remarkably successful, existing theoretical models (Madsen and Svendsen, 1981; McCorquodale and Khalifa, 1983; Svendsen and Kirby, 2004) are capable of approximating the velocity distribution in the vertical direction, the free surface location, and the length of hydraulic jumps, but they are unable of providing either the details of turbulence or the incorporation of air at the free surface. Recent interesting numerical results (Stelling and Busnelli, 2001; Ma et al., 2002), show satisfactory predictions of mean flow and turbulence, but they have ignored the two-phase nature of the flow and the associated air entrainment. Ma et al. (2002) stated in their efficient, recent numerical simulation of a submerged hydraulic jump that "it is expected that the inclusion of air entraining, the effect of streamline curvature and more accurate free

surface conditions for turbulent quantities...would improve the numerical calculation of hydraulic jumps significantly.”

The objective of this paper is to characterize mean flow and air entrainment in hydraulic jumps through numerical means (**FLOW-3D<sup>®</sup>**), in three dimensions, using the one-phase flow theory. In this endeavor, the code does not incorporate any assumption about hydrostaticity (i.e., “streamline curvature” is considered explicitly), it embeds a very accurate treatment for the free surface through the true VOF (volume-of-fluid) method. The global aim of this work is to obtain a set of validated turbulent model for hydraulic jumps for different Froude numbers.

## 2 Aerated Flow Mathematical Model

### 2.1 Time Averaged Flow Equations

The general mass continuity equation is [8]:

$$V_f \frac{\partial \rho}{\partial t} + \frac{\partial}{\partial x}(\rho u A_x) + \frac{\partial}{\partial y}(\rho v A_y) + \frac{\partial}{\partial z}(\rho w A_z) = 0 \quad (1)$$

Where  $V_f$  is the fractional volume open to flow,  $\rho$  is the fluid density. The velocity components ( $u, v, w$ ) are in the coordinate directions ( $x, y, z$ ).  $A_x, A_y$  and  $A_z$  are similar area fractions for flow in the  $x, y$  and  $z$  directions, respectively.

The equation of motion for the fluid velocity components in the three directions are the Navier – Stokes equations as follows [8]:

$$\frac{\partial u}{\partial t} + \frac{1}{V_f} \left\{ u A_x \frac{\partial u}{\partial x} + v A_y R \frac{\partial u}{\partial y} + w A_z \frac{\partial u}{\partial z} \right\} = -\frac{1}{\rho} \frac{\partial p}{\partial x} + G_x + f_x \quad (2)$$

$$\frac{\partial v}{\partial t} + \frac{1}{V_f} \left\{ u A_x \frac{\partial v}{\partial x} + v A_y R \frac{\partial v}{\partial y} + w A_z \frac{\partial v}{\partial z} \right\} = -\frac{1}{\rho} \left( R \frac{\partial p}{\partial y} \right) + G_y + f_y \quad (3)$$

$$\frac{\partial w}{\partial t} + \frac{1}{V_f} \left\{ u A_x \frac{\partial w}{\partial x} + v A_y R \frac{\partial w}{\partial y} + w A_z \frac{\partial w}{\partial z} \right\} = -\frac{1}{\rho} \frac{\partial p}{\partial z} + G_z + f_z \quad (4)$$

In these equations  $G_x, G_y, G_z$  are body accelerations, and  $f_x, f_y, f_z$  are viscous accelerations that for a variable dynamic viscosity  $\mu$  are as follows:

$$\rho V_f f_x = w s x - \left\{ \frac{\partial}{\partial x} (A_x \tau_{xx}) + R \frac{\partial}{\partial y} (A_y \tau_{xy}) + \frac{\partial}{\partial z} (A_z \tau_{xz}) + \frac{\xi}{x} (A_x \tau_{xx} - A_y \tau_{xy}) \right\} \quad (5)$$

$$\rho V_f f_y = w s y - \left\{ \frac{\partial}{\partial x} (A_x \tau_{xy}) + R \frac{\partial}{\partial y} (A_y \tau_{yy}) + \frac{\partial}{\partial z} (A_z \tau_{yz}) + \frac{\xi}{x} (A_x + A_y \tau_{xy}) \right\} \quad (6)$$

$$\rho V_f f_z = w s z - \left\{ \frac{\partial}{\partial x} (A_x \tau_{xz}) + R \frac{\partial}{\partial y} (A_y \tau_{yz}) + \frac{\partial}{\partial z} (A_z \tau_{zz}) + \frac{\xi}{x} (A_x \tau_{xz}) \right\} \quad (7)$$

Where:

$$\tau_{xx} = -2\mu \left\{ \frac{\partial u}{\partial x} - \frac{1}{3} \left( \frac{\partial u}{\partial x} + \frac{\partial v}{\partial y} + \frac{\partial w}{\partial z} \right) \right\} \quad (8)$$

$$\tau_{yy} = -2\mu \left\{ \frac{\partial v}{\partial y} - \frac{1}{3} \left( \frac{\partial u}{\partial x} + \frac{\partial v}{\partial y} + \frac{\partial w}{\partial z} \right) \right\} \quad (9)$$

$$\tau_{zz} = -2\mu \left\{ \frac{\partial w}{\partial z} - \frac{1}{3} \left( \frac{\partial u}{\partial x} + \frac{\partial v}{\partial y} + \frac{\partial w}{\partial z} \right) \right\} \quad (10)$$

$$\tau_{xy} = -\mu \left\{ \frac{\partial v}{\partial y} + \frac{\partial u}{\partial x} \right\} \quad (11)$$

$$\tau_{xz} = -\mu \left\{ \frac{\partial u}{\partial z} + \frac{\partial w}{\partial x} \right\} \quad (12)$$

$$\tau_{yz} = -\mu \left\{ \frac{\partial v}{\partial z} + \frac{\partial w}{\partial y} \right\} \quad (13)$$

### 2.2 Free Surface Trace Equation

Free surface boundary configuration of the flow is defined in terms of a volume of fluid (VOF) function,  $F(x, y, z$  and  $t$ ). This function represents the volume of fluid per unit volume and satisfies the equation [8].

$$\frac{\partial F}{\partial t} + \frac{1}{V_f} \left[ \frac{\partial}{\partial x} (F A_x u) + \frac{\partial}{\partial y} (F A_y v) + \frac{\partial}{\partial z} (F A_z w) \right] = 0 \quad (14)$$

The interpretation of  $F$  depends on the type of problem being solved. For a single fluid,  $F$  represents the volume fraction occupied by the fluid. Thus fluid exists where  $F=1$  and void regions correspond to locations where  $F=0$ . Voids are regions without fluid mass that have a uniform pressure assigned to them. Physically they represent regions filled with a vapor or gas whose density is insignificant with respect to fluid density.

### 2-3 Air Entrainment Relations

Air entrainment at a liquid surface is based on the idea that turbulent eddies raise small liquid elements above a free surface that may trap air and carry it back into the body of the liquid. The extent to which liquid elements can be lifted above a free surface depends on whether or not the intensity of the turbulence is enough to overcome the surface stabilizing forces of gravity and surface tension.

Turbulence transport models characterize turbulence by a specific turbulent kinetic energy  $Q$  and a dissipation function  $D$ . A characteristic size of turbulence eddies is then given by  $L_t = c n u (3/2)^{1/2} Q^{3/2} D$ . We use this scale to characterize surface disturbances. The disturbance kinetic energy per unit volume (i.e., pressure) associated with a fluid element raised to a height  $L_t$  and with surface tension energy based on a curvature of  $L_t$  is  $P_d = \rho g_n L_t + \frac{\sigma}{L_t}$ . Here  $\rho$  is the liquid

density,  $\sigma$  its coefficient of surface tension, and  $g_n$  is the component of gravity normal to the free surface.

For air entrainment to occur the turbulent kinetic energy per unit volume,  $P_t = \rho Q$ , must be larger than  $P_d$ , i.e., the turbulent disturbances must be large enough to overcome the surface stabilizing forces.

The volume of air entrained per unit time,  $\delta V$ , should be proportional to the surface area,  $A_s$ , and the height of the disturbances above the mean surface level. All together we write  $\delta V = C_{air} A_s \sqrt{(2(P_t - P_d)/\rho)}$ , where  $C_{air}$  is a coefficient of proportionality. If  $P_t$  is less than  $P_d$  then  $\delta V$  is zero. The value of  $C_{air}$  is expected to be less than unity, because only a portion of the raised disturbance volume is occupied by air. A good first guess is  $C_{air} = 0.5$ , i.e., assume on average that air will be trapped over about half the surface area. [2].

### 3 Turbulent Models

Two turbulent models are used in present numerical investigations and their results are compared with the experimental observations and measurements in the next sections.

#### 3.1 $k-\varepsilon$ turbulent model

The simplest model consists of a transport equation for the specific kinetic energy associated with turbulent velocity fluctuations plus a parameter that characterizes some other property of the turbulence. The choice of parameters is arbitrary provided it can be used with the kinetic energy to determine length and time scales characterizing the turbulence.

A slightly more sophisticated (and more widely used) model consists of two transport equations for the turbulent kinetic energy  $k$  and its dissipation  $\varepsilon$ , the so-called  $k-\varepsilon$  model [9]. The  $k-\varepsilon$  model has been shown to provide reasonable approximations to many types of flows, although it sometimes requires modification of its dimensionless parameters (or even functional changes to terms in the equations) [13]. The turbulence kinetic energy,  $k$ , and its rate of dissipation,  $\varepsilon$ , are obtained from the following transport equations:

$$\frac{\partial k}{\partial t} + \frac{1}{V_f} \left\{ u A_x \frac{\partial k}{\partial x} + v A_y \frac{\partial k}{\partial y} + w A_z \frac{\partial k}{\partial z} \right\} = P + G + Diff - \varepsilon \quad (15)$$

$$\frac{\partial \varepsilon}{\partial t} + \frac{1}{V_f} \left\{ u A_x \frac{\partial \varepsilon}{\partial x} + v A_y \frac{\partial \varepsilon}{\partial y} + w A_z \frac{\partial \varepsilon}{\partial z} \right\} = \frac{C_{1\varepsilon} \varepsilon}{k} (P + C_{3\varepsilon} G) + DDif - C_{2\varepsilon} \frac{\varepsilon^2}{k} \quad (16)$$

Where,  $P$  is shear production,  $G$  is buoyancy production,  $Diff$  and  $DDif$  represent diffusion and  $C_{1\varepsilon}$ ,  $C_{2\varepsilon}$ ,  $C_{3\varepsilon}$  are constant. In standard  $k-\varepsilon$  model  $C_{1\varepsilon} = 1.44$  and  $C_{2\varepsilon} = 1.92$ .

#### 3.2 RNG turbulent model

Another, more recent turbulence model is based on Renormalization-Group (RNG) methods [17, 18]. This approach applies statistical methods for a derivation of the averaged equations for turbulence quantities, such as turbulent kinetic energy and its dissipation rate. The RNG-based models rely less on empirical constants while setting a framework for the derivation of a range of models at different scales.

The RNG model uses equations similar to the equations for the  $k-\varepsilon$  model. However, equation constants that are found empirically in the standard  $k-\varepsilon$  model are derived explicitly in the RNG model.

Generally, the RNG model has wider applicability than the standard  $k-\varepsilon$  model. In particular, the RNG model is known to describe more accurately low intensity turbulence flows and flows having strong shear regions.

In RNG model  $C_{1\varepsilon} = 1.42$  and  $C_{2\varepsilon} = 1.68$ .

### 4 Numerical Solution Techniques

**FLOW-3D**<sup>®</sup> numerically solves the equations described in the previous sections using finite-volume approximations. The flow region is subdivided into a mesh of fixed rectangular cells. With each cell there are associated local average values of all dependent variables. All variables are located at the centers of the cells except for velocities, which are located at cell faces (staggered grid arrangement).

Curved obstacles, wall boundaries, or other geometric features are embedded in the mesh by defining the fractional face areas and fractional volumes of the cells that are open to flow (the FAVOR<sup>™</sup> method).

Pressures and velocities are coupled implicitly by using time-advanced pressures in the momentum equations and time-advanced velocities in the mass (continuity) equation [8]. This semi-implicit formulation allows for the efficient solution of low speed and incompressible flow problems. The semi-implicit formulation, however, results in coupled sets of equations that must be solved by an iterative technique. In **FLOW-3D**<sup>®</sup> two such techniques are provided. The simplest is a successive over-relaxation (SOR) method [8]. In some instances, where a more implicit solution method is required, a special alternating-direction, line-implicit method (SADI) is available [8]. The SADI technique can be

used in one, two, or in all three directions depending on the characteristics of the problem to be solved.

The basic numerical method used in *FLOW-3D*<sup>®</sup> has a formal accuracy that is first order with respect to time and space increments. Special precautions have been taken to maintain this degree of accuracy even when the structured mesh is non-uniform.

A new VOF advection method based on a 3-D reconstruction of the fluid interface has been developed and implemented in *FLOW-3D*<sup>®</sup> Version 8.2. The Volume-of-Fluid (VOF) function is moved in one step, without resorting to an operator splitting technique, which gives the present method increased accuracy when the flow is not aligned with a coordinate direction [8].

The existing VOF advection method in *FLOW-3D*<sup>®</sup> is based on the donor-acceptor approach first introduced by Hirt and Nichols [8].

## 5 Verification Tests

### Hydraulic jump

In this section, the experimental data for velocity profiles obtained from the plots provided by H. Chanson and T. Brattberg (2000) are used for verification of numerical results.

The experiments were performed in a 3.2-m long horizontal channel of uniform rectangular section (Chanson and Qiao, 1994; Chanson, 1995a), the flume was 0.25-m wide, the sidewalls are 0.30-m high and both walls and bed were made of glass. Regulated flows were supplied through an adjustable vertical sluice gate. During the experiments, the gate opening was fixed at 20 mm.

The model boundary condition for this case, with sub-critical flow occurring at upstream boundary, with is specified upstream depth ( $h_0$ ) and vanishing derivatives of extra pressure and velocity variables. As downstream flow is sub-critical, and water surface conditions are applied at downstream end. The  $k-\varepsilon$  and RNG models are used for turbulence modeling. Mesh of constant density was employed until the numerical results were invariant in terms of mean flow and turbulence statistics. The grid size corresponds to  $5 \times 5 \times 5$  mm.

Figures 1 and 3 show the computed  $x$  direction velocity component, pressure contours model and resulted velocity profiles at different locations of the hydraulic jump. The computed results obtained using  $k-\varepsilon$  and RNG turbulent models are compared with Chanson and Brattberg (2000) observations in Figures 2 and 4. The general agreement between predicted and measured profiles produced by RNG

turbulent model is satisfactory. However, because of highly aerated turbulent flow in the upper zone of hydraulic jump, there are poor agreements between computed and measured velocity values.

### Transition from hydraulic jump to open channel flow

This section presents the results of numerical study on the transition from the end of the surface roller to the section where the velocity profiles resemble those of fully developed turbulent open channel flow.

Boundary and initial conditions were set in the model in order to mimic the experimental set up used by S. Wu and N. Rajaratnam (1996). These experiments were performed in a horizontal flume 7.6 m long, 0.466 m wide and 0.6 m high. The supercritical stream was 16.5 mm and the jumps were formed at the gate.

A 3-D mesh with 16000 cells is applied for numerical simulation. The water flow enters the calculation domain with 16.5 mm depth, 1.56 m/s velocity and 3.87 froude number. As downstream flow is sub-critical, and water surface conditions are applied at downstream end. The  $k-\varepsilon$  and RNG models are used for turbulent modeling of aerated flow solution. Mesh of constant density was employed until the numerical results were converged in terms of mean flow and turbulence statistics.

Figures 5 and 7 show the compute  $x$  direction velocity, pressure contours and Figures 6, 8 shows the comparison between measured  $x$ -velocity profiles for different distance from toe of jump and compute results of  $k-\varepsilon$  and RNG turbulent models.

The general trend of transition of horizontal velocity profile form hydraulic jump to open channel is better computed using RNG turbulent model rather than the  $k-\varepsilon$  turbulent model. However downstream of the hydraulic jump, similar results are produced by both turbulence models and present good agreements with measured data.

## 6 Conclusion

In this paper numerical investigations are performed for evolution of the ability of an available 3D flow solver to cop with the fully turbulent aerated flow with free surface in transition from super-critical to sub-critical flow. In this work *FLOW-3D*<sup>®</sup> finite volume flow solver which is utilized with VOF technique for free surface modeling is used. The results of numerical experiments of two turbulent modeling options of the software; RNG and  $k-\varepsilon$  two equation models are used in this paper. The

comparison of the computed results of two test cases of aerated hydraulic jumps with the reported experimental measurements shows that:

The CFD code can efficiently forecast the general trend of transformation of three dimensional velocity patterns to the horizontal velocity field.

In aerated hydraulic jumps zone, the x direction velocity trend forecasted by the RNG turbulent model present better agreement with the measured data, rather than the results produced with the  $k-\varepsilon$  turbulent model. At the lower zones of the aerated hydraulic jump the trends of computed x direction velocity component is very similar to the experimental data, while the computed profiles x direction velocity differ from measured data at the upper parts of aerated hydraulic jumps. However, the velocity fields computed using RNG turbulent model are slightly less than the experimental measurements at all sections in the stilling basin.

The computed results obtained by the use of both turbulent models are more accurate in fully developed flow down stream of the hydraulic jump, rather than the results obtained for the aerated flow patterns in hydraulic jumps zone. However, in the sub-critical flow zone down stream of the hydraulic jump the difference between the x direction velocity profiles computed by both turbulent models are less than the differences in the aerated hydraulic jump zone.

#### References:

- [1] C.W. Hirt and B.D. Nichols, "Volume of Fluid (VOF) Method for the Dynamics of Free Boundaries", *J. Comp. Phys.*, Vol. 39, 1981, pp.201-225.
- [2] C.W. Hirt, "Modeling Turbulent Entrainment of Air at a Free Surface", *Flow Science, Inc.*, 2003, FSI-03-TN61.
- [3] Chanson H., Brattberg T., "Experimental study of the air-water shear flow in hydraulic jump", *International Journal of Multiphase Flow*, Vol.26, 2000, pp. 583-607.
- [4] Chanson, H., "Air bubble entrainment in free-surface turbulent flows" *Experimental investigations. Report CH46/95, Department of Civil Engineering, University of Queensland, Australia*, June 1995, 368.
- [5] Chanson, H., "Air Bubble Entrainment in Free-surface Turbulent Shear Flows", *Academic Press, London, UK*, 1997, p. 401.
- [6] Chanson, H., "Air entrainment in two-dimensional turbulent shear flows with partially developed inflow conditions", *Int. J. of Multiphase Flow* 21 (6), 1995, 1107±1121.
- [7] Chanson, H., Qiao, G.L., "Air bubble entrainment and gas transfer at hydraulic jumps", Research Report No. CE149, Department of Civil Engineering, University of Queensland, Australia, August 1994, 68.
- [8] **FLOW-3D**<sup>®</sup> user manual, Ver. 9.0.
- [9] Harlow F.H. and Nakayama P.I., "Turbulence Transport Equations", *Phys. of Fluids*, 10, 1967, 2323.
- [10] Madsen, P. and Svendsen, I. "Turbulent bores and hydraulic jumps", *J. Fluid Mech.*, 129, 1983, pp. 1-25.
- [11] McCorquodale, J. and Khalifa, A., "Internal flow in hydraulic jumps", *J. Hyd. Eng.*, 109, 1981, pp. 684-701.
- [12] Resch, F.J., Leutheusser, H.J., Le ressaut hydraulique: mesure de turbulence dans la region diphasique. (The hydraulic jump: turbulence measurements in the two-phase flow region.), *J. La Houille Blanche*, (4), 1972, 279±293 (in French).
- [13] W. Rodi, "Turbulence Models and Their Application in Hydraulics - A State of the Art Review", *International Association of Hydraulic Research publication*, 1980.
- [14] Svendsen, I. and Kirby, J., "Numerical study of a turbulent hydraulic jump," *Proc. 17th ASCE Engineering Mechanics Conference*, University of Delaware, Newmark, DE, 2004.
- [15] Wood, I.R., "Air entrainment in free-surface flows", *IAHR Hydraulic Structures Design Manual*, No. 4, Hydraulic Design Considerations. Balkema, Rotterdam, the Netherlands, 1990, p. 149.
- [16] Wu. S., Rajaratnam N., "Transition from Hydraulic Jump to Open Channel Flow", *J. Hydraulic engineering*, Vol. 122, No.9, 1996, pp. 526-528.
- [17] Yakhot V. and Orszag S.A., "Renormalization Group Analysis of Turbulence. I. Basic Theory", *J. Scientific Computing*, 1, 1986, pp. 1-51.
- [18] Yakhot V. and Smith L.M., "The Renormalization Group, the e-Expansion and Derivation of Turbulence Models", *J. Scientific Computing*, 7, 1992, pp. 35-61.

Figures

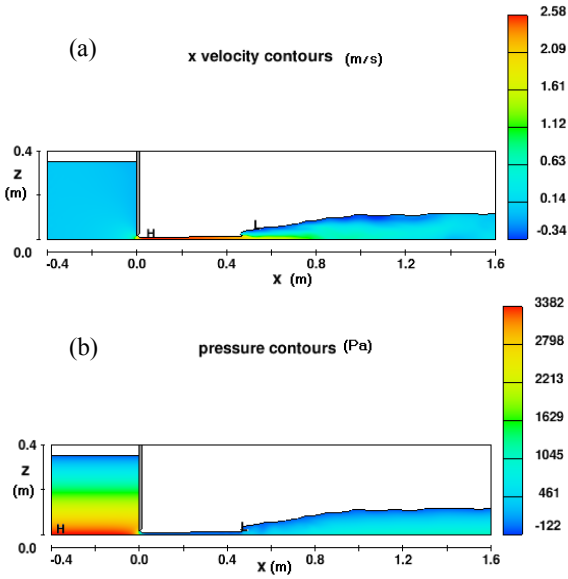


Fig. 1, (a) x direction velocity and (b) Pressure contours for F=6.33 and RNG model

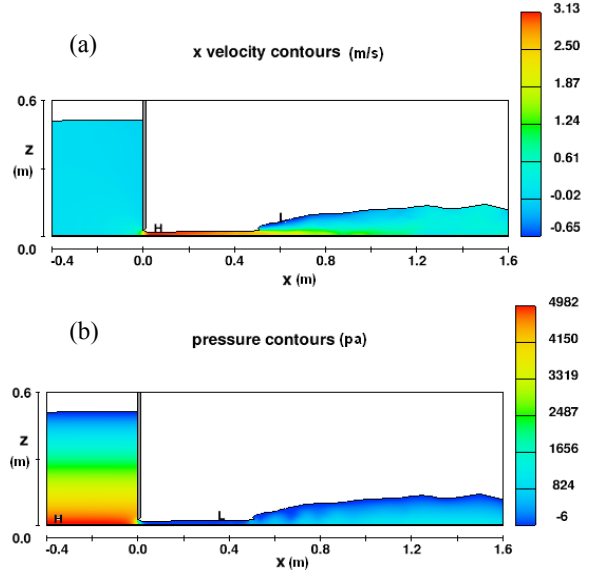


Fig. 3, (a) x direction velocity and (b) Pressure contours for F=8.48 and RNG model

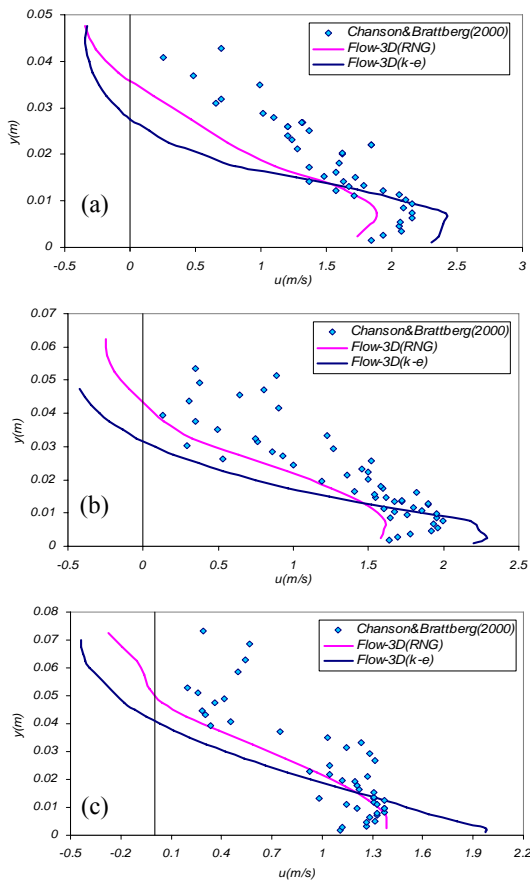


Fig. 2, x-velocity profile at (a) 0.05 m, (b) 0.1 m, (c) 0.2 m from toe of jump for F=6.33

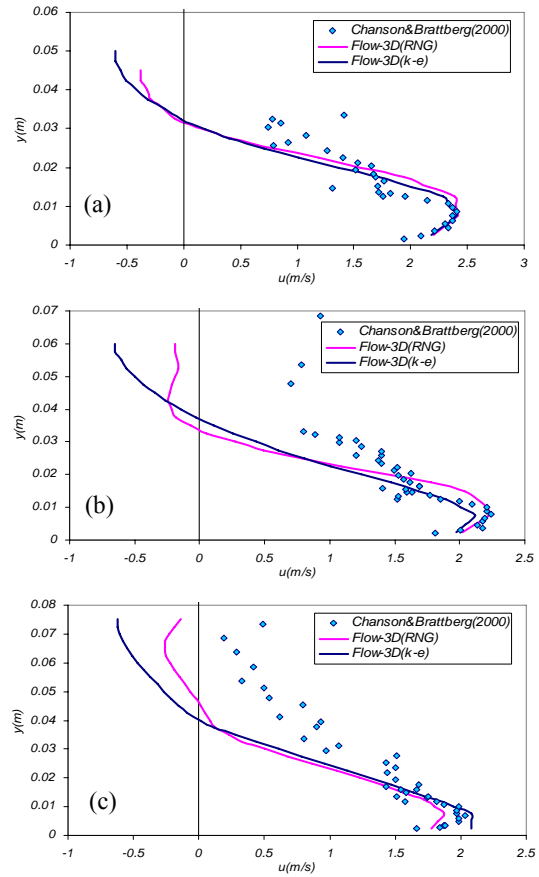


Fig. 4, x-velocity profile at (a) 0.05 m, (b) 0.1 m, (c) 0.2 m from toe of jump for F=8.48

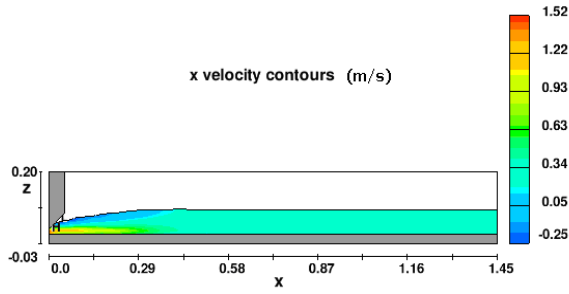


Fig. 5, x-velocity contours for RNG model

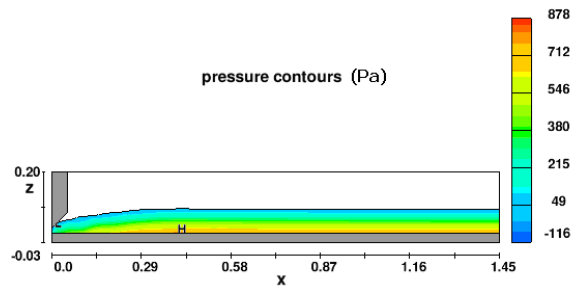


Fig. 7, Pressure contours for RNG model

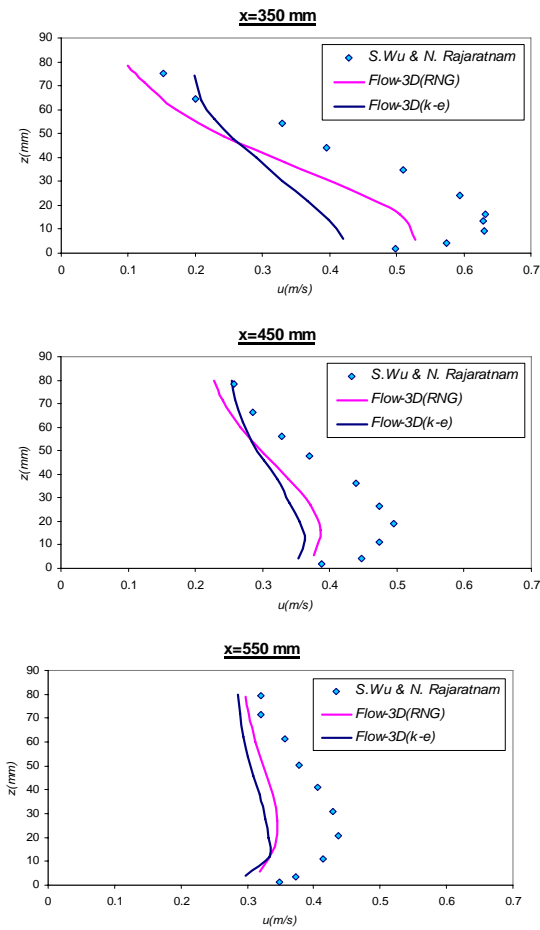


Fig. 6, x-velocity profile at 350 mm, 450 mm, 550 mm, from toe of jump

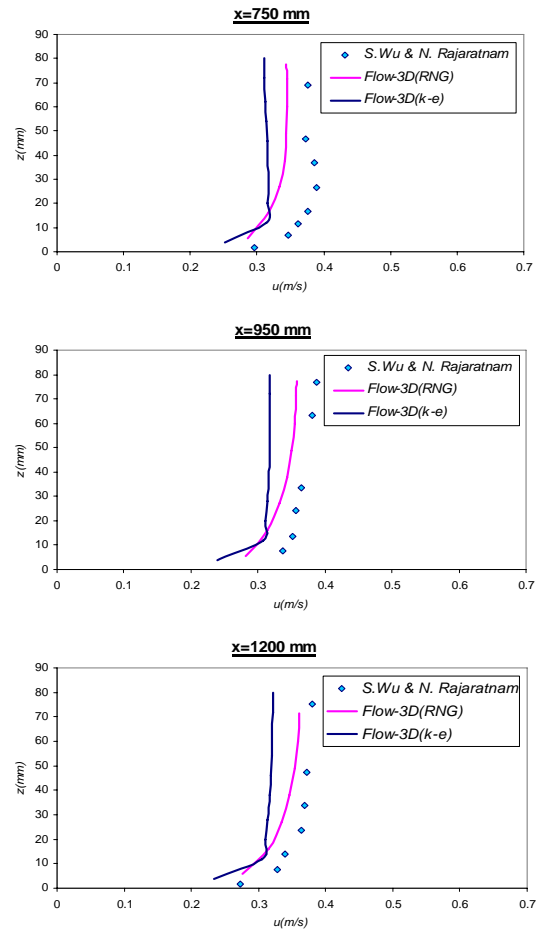


Fig. 8, x-velocity profile at 750 mm, 950 mm, 1200 mm, from toe of jump